LAWRENCE
LIVERMORE
NATIONAL
LABORATORY

LLNL-SR-739549

Subcontract Report: Diffusion Mechanisms and Bond Dynamics in Solid Electrolyte Ion-Conductors

A. Zevgolis, A. Hall, T. Alvez, Z. Mehmedovic, P. Shea, J. Varley, B. C. Wood, N. Adelstein

October 5, 2017

Disclaimer

This work performed under the auspices of the U.S. Department of Energy by Lawrence Livermore National Laboratory under Contract DE-AC52-07NA27344.

SAN FRANCISCO STATE UNIVERSITY

Office of Research and Sponsored Programs
1600 Holloway Avenue, ADM 471
San Francisco, California 94132
Tel: 415/338-7094
Fax: 415/338-2493

Date: **09/29/2017**
PI Name: Nicole Adelstein
Project #: 60481000
Sponsor: Lawrence Livermore National Laboratory
Title: **Diffusion Mechanisms and Bond**
Dates: **11/21/2016 to 09/30/2017**

Please find the enclosed report of work performed for Lawrence Livermore National Laboratory.

Sincerely,
Nicole Adelstein

Bond Frustration and Nano-Phase Separation in Lithium Indium Halides

Alysia Zevgolis, Alex Hall, Thomaz Alvez, Zerina Mehmedovic, Patrick Shea§, Joel Varley§, Brandon Wood§, and Nicole Adelstein

§ Materials Science Division, Lawrence Livermore National Laboratory, Livermore, CA 94550, USA
§§ Department of Chemistry and Biochemistry, San Francisco State University

Abstract

We employ first-principles molecular dynamics simulations and Maximally Localized Wannier Function (MLWF) analysis to explore how halide substitution and nano-phase microstructures affect diffusivity, through the activation energy barrier - E_a and D_0, in the solid electrolyte $Li_3InBr_{6-x}Cl_x$. We find that nano-phase microstructures with x=3 (50-50 Br-Cl) mixed composition have a higher diffusivity compared to x=2 and x=3 solid solutions. There is a positive linear relationship between ln(D_0.) and E_a, which suggests that for superionic conductivity optimizing both the activation energy and the D_0 is important. Bond frustration due to mismatch in crystal geometry and ideal coordination number leads to especially high diffusivity through a high D_0 in the x=3 composition.

Introduction

There is building consensus that frustration, the inability for a system with mobile ions to settle in a significantly deep energy minimum, contributes to superionic conductivity. Examples of superionic electrolytes for lithium ion batteries (LIBs) includes garnets[1-3], NASICON[4-6], anti-perovskites[7-8], LGPS[9], and our recent work on Li_3InBr_6[10]. Ab-*initio* simulation of Li_3InBr_6 revealed the bonds between Li and the anion lattice fluctuated between very ionic to more polar-covalent character. The bond character fluctuates faster than Li diffusion, in part because Br in an octahedral site cannot optimize a tetrahedral coordination of Li cations with significant polar-covalent character in all four Li-Br bonds. If a polar-covalent bond is formed between Br and Li, then a different Br-Li bond may become more ionic and Li may diffuse, setting up a chain of correlated diffusion events. This chain of correlated diffusion events caused by bond frustration contributes to Li_3InBr_6's high diffusion and conductivity (10^{-3} S cm^{-1}).

Our analysis of diffusivity in $Li_3InBr_{6-x}Cl_x$ confirms the contribution of polar-covalent bonds to superionic behavior in these halide-based electrolytes. According to Fajan's[11] rules, the Br-Li bond is expected to have more polar-covalent character compared to Cl-Li bonds. We characterize the polar-covalent bond of these Li-halide bonds by calculating the electron density and projecting it onto "orbitals", Maximally Localized Wannier Functions (MLWF), that serve as a proxy for bonds. We found that the more polar-covalent character of the Li-Br bonds contributes to a higher maximum diffusion coefficient, D0.

$Li_3InBr_{6-x}Cl_x$ has an unusual, non-monotonic trend in conductivity with Cl substitution that could not be completely explained by differences in Br-Li and Cl-Li bond character. Our molecular dynamics simulation of four different compositions did not match the experimental trend at 500 K. We found that the unusually high conductivity of half Cl-half Br system is likely due to a nano-phase separation of Br-rich regions and Cl-rich regions. The results presented in this paper show an increased conductivity in a nano-phase separated material as compared to the solid solution.

This paper is organized as follows: the unusual conductivity trend in $Li_3InBr_{6-x}Cl_x$ (hence-forth called the mixed halide system) is presented in the computational details section. Then, the simulation results are presented separated from detailed analysis of the character of the bonds and their effect on frustration and diffusion in the discussion section.

Computational details

We compare the simulated diffusivity Li_3InBr_6, $Li_3InBr_4Cl_2$, $Li_3InBr_3Cl_3$, Li_3InCl_6, to discover the cause of the different conductivity at various levels of Cl-substitution. This work expands our previous study into Li_3InBr_6[10] and confirms the importance of Li-anion bond character and frustration in superionic conductivity in this system. We simulate the effect of microstructure on diffusivity in the half Br-half Cl composition using two supercells: one a solid-solution and the other nano-phase separated. We were inspired to simulate the nano-phase separated supercell due to the hysteresis in volume upon Cl substitution (Fig. 1), the XRD (not shown), and unusual NMR (not shown)

signature at this composition.[20] Figure 1 shows that Br-rich compositions and Cl-rich compositions follow different trends of volume versus composition. However, some of the Cl-rich compositions follow the trend of volume in the more Br-rich systems, while other samples follow the Cl-rich trend line. Sampels with two different volumes indicate different microstructures and the XRD indicates a phase-separation at the x=3 composition. The NMR shows the x=3 system has unusually high conductivity.

First-principles Børn-Oppenheimer molecular dynamics[13] simulations were run on 2x2x2 supercells of $Li_3InBr_{6-x}Cl_x$ using the Quantum ESPRESSO plane-wave density functional theory code.[14] A time step of 20 a.u. (0.97 fs), and wavefunction and charge density cutoffs of 30 Ry and 300 Ry were used after convergence tests were run. Ultrasoft pseudopotentials[15] for Li, In, Cl, and Br were employed with the Perdew-Burke-Ernzerhof (PBE) exchange-correlation functional.[16] The pseudopotentials are Li.pbe-s-van_ak.UPF, In.pbe-d-rrkjus.UPF, Cl.pbe-n-van.UPF, and Br.pbe-van_mit.UPF.

The four ratios of Br to Cl were simulated at various volumes at temperatures, henceforth termed Br/Cl compositions. A short hand will also be employed to refer to the simulated Br/Cl compositions: $Li_3InBr_6 = Br_6$, $Li_3InBr_4Cl_2 = Br_4$, $Li_3InBr_3Cl_3 = Br_3$, and $Li_3InCl_6 = Cl_6$. These systems were simulated as solid solutions with a random placement of Br and Cl in the supercell and the lowest energy configuration of at least three configurations tested for Br_3 and Br_4 was simulated. In addition, a nano-phase (NP) separated supercell with a Cl-rich side and Br-rich side was simulated for the Br_3 composition (see Figure 2). Table 1 gives our optimized lattice vectors for each supercell.

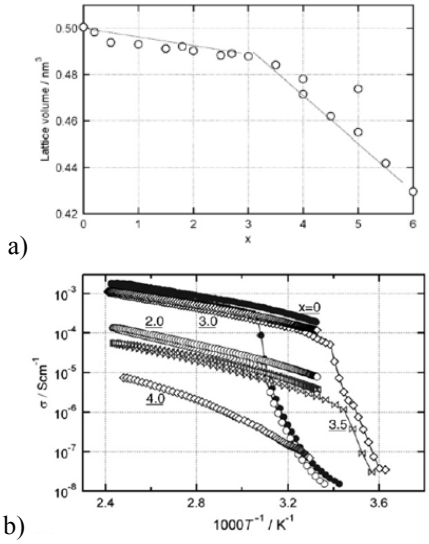

Figure 1. $Li_3InBr_{6-x}Cl_x$ at 500 K a) *x* is increasing Cl substitution for Br. a) Lattice volume of $Li_3InBr_{6-x}Cl_x$. b) temperature dependence of AC conductivity.[12]

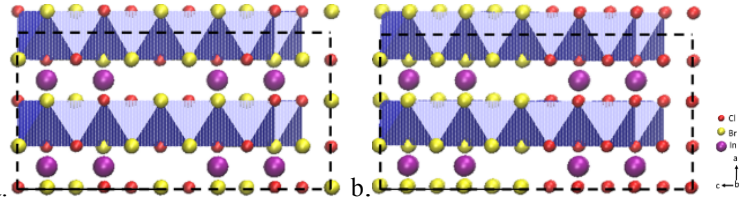

Figure 2. 2x2x2 supercell of $Li_3InBr_3Cl_3$ in a) solid solution and b) nanophase separation. Blue octahedrons represent Li bound to six halides. Cl, Br and In are shown as red, yellow, and purple. Black dashed lines indicate 2x2x2 unit cell in 'ca' plane.

Table 1. Computationally optimized lattice vectors for 2x2x2 supercells with ɣ = 109.3° At an expanded volume of 4389 Å^3, the shape of the supercell was optimized for the mixed halides$^+$. The optimized lattice vectors at the optimized volume for Li_3InBr_6 is given in the second column*.

Optimize	Br_6	large $Br_{4/3}$	Br_4	Br_3	Cl_6
Vol. (Å^3)	4389	4389	4262	4112	3638
a = b (Å)	13.44	14.07	13.94	13.66	13.13
c (Å)	25.74	23.95	23.72	23.40	22.54

Simulations were run at 500 K, 700 K, 800 K, and 900 K, with temperatures maintained with the canonical (NVT) dynamics ensemble using velocity rescaling set within the Quantum ESPRESSO code.[14] Each simulation was run for at least 25 ps following an initial equilibration period.

Maximally Localized Wannier Functions (MLWF) were calculated at 48 fs intervals over 930 frames for each simulation. MLWFs were constructed using the Wannier90 code.[17, 18, 19] The wavefunctions were initialized by projecting the electron density onto an s orbital for Li, an sp3 orbital for Br/Cl, and d orbitals for In. The projection was considered maximally localized if the change in the spread between iterations was less than 1 x 10^{-6} Å^2.[10]

Li^+ ions in each simulation frame were separated according to “jumping" Li^+ that are actively involved in an octahedral-to-octahedral site jump (typically via an intermediate tetrahedral site) and “ordinary" Li^+ that encompasses all Li^+, as in our previous work.[10] We require the jumps to complete within 430 fs, to ensure jumps are individual diffusion events, rather than sequential processes.

Results

Diffusion coefficients and activation energy barriers (Tables 2 and 3) were calculated for four compositions: Li_3InBr_6, $Li_3InBr_4Cl_2$, $Li_3InBr_3Cl_3$, Li_3InCl_6 at temperatures 500-900 K; and, for the mixed compositions, at volumes 4112 Å^3, 4262 Å^3, and 4389 Å^3.

Table 2. Diffusion coefficients for solid solutions $Li_3InBr_{6-x}Cl_x$

	Temp (K)	4389 Å^3	4262 Å^3	4112 Å^3	3638 Å^3
Li_3InBr_6 / Li_3InCl_6	500	7.234E-6	-	-	2.291E-6
	700	8.170E-6	-	-	1.128E-5
	800	2.833E-5	-	-	1.390E-5
	900	2.895E-5	-	-	1.952E-5
$Li_3InBr_4Cl_2$	500	3.717E-6	3.884E-6	8.767E-7*	-
	700	1.450E-5	1.068E-5	8.092E-7	-
	800	2.744E-5	1.443E-5	1.242E-5	-
	900	3.473E-5	2.925E-5	1.478E-5	-
$Li_3InBr_3Cl_3$	500	6.741E-6	2.503E-6	2.696E-6	-
	700	1.704E-5	1.889E-5	9.909-6	-
	800	4.580E-5	3.379E-5	1.815E-5	-
	900	4.897E-5	3.730E-5	3.626E-5	-

* simulated at 650 K

Table 3. Maximum diffusion coefficients and E_a for simulations 500-800K

	4389/ 3638** Å^3		4262 Å^3		4112 Å^3	
	D_o (cm^2/s)	E_a (eV)	D_o (cm^2/s)	E_a (eV)	D_o (cm^2/s)	E_a (eV)
Li_3InBr_6/ Li_3InCl_6	1.22E-4 2.65E-4	0.127 0.194	-	-	-	-
$Li_3InBr_4Cl_2$	6.53E-4	0.224	1.30E-4	0.151	2.46E+3	1.3
$Li_3InBr_3Cl_3$	6.49E-4	0.200	2.69E-3/ 3.08E-4**	0.300/ 0.184**	3.75E-4	0.214

*volume used for Li_3InCl_6 only
**E_a and D_0 for $Li_3InBr_3Cl_3$ with nanophase separation

Order in Ea: Br6, Br4, Cl6, Br3. Order in D0: Br3,Cl6, Br4,Br6. Order in D at 500K: Br6, Br4, Br3, Cl6. The trend in diffusion coefficients at 500 K (Br6, Br4, Br3, Cl6) does not match the experimental trend in conductivity around 500 K (Br6, Br3, Br4, Cl6), as seen in Table 2. The Br4 solid solution has a higher diffusivity than the Br3 at 500 K due to its lower activation energy barrier.

The experimental trend in conductivity can be modelled by assuming a nano-phase microstructure of the Br3 composition. The nano-phase microstructure (NP) has significantly higher diffusivity at 700 K in the small cell and we assume this trend would hold at 500 K because the NP has a significantly lower activation energy barrier.

The activation energy barrier is calculated using the Arrhenius expression for diffusion coefficient, *D*:

$$D = D_0 e^{\frac{-E_a}{k_B T}}$$

where E_a is the activation energy barrier, k_B is the Boltzmann's constant, T is the temperature and D_0.

Through our analysis we noted that the medium volume simulations of Br3 show the largest D_0, because bond frustration is maximized. Thus, we chose to simulate the NP at the medium volume at multiple temperatures to assess how the microstructure affected the frustration. At 800 K and 900 K for the medium volume, the solid solution has a higher diffusivity, *D*, than the NP, because D_0 is so high for the mid-volume solid solution Br3. Across all our simulations, the material (composition and volume) with higher diffusivity often changes at higher temperatures due to non-Arrhenius behavior. Non-Arrhenius behavior indicates two different activation energy barriers with different diffusion processes. The activation energy barrier does not change at the same temperature for all the different simulations. However, the non-Arrhenius behavior often occurs at between 800 K and 900 K, so we report activation energy barriers between 500-800 K in Table 3 and 4.

Table 4. Diffusion coefficients for NP $Li_3InBr_3Cl_3$

	Temp (K)	4389Å^3	4262 Å^3	4112 Å^3
Nanophase Separation $Li_3InBr_3Cl_3$ E_a = 0.13 eV D_0 = 2.0E-4 cm^2/s	**500**	-	3.803E-06	-
	700	2.552E-05	1.075E-05	1.105E-05
	800	-	2.545E-05	-
	900	-	4.021E-05	-
Solid Solution $Li_3InBr_3Cl_3$ E_a = 0.28 eV D_0 = 1.5E-3 cm^2/s	**500**	6.741E-06	2.503E-06	2.696E-06
	700	1.704E-05	1.889E-05	9.909E-06
	800	4.580E-05	3.379E-05	1.815E-05
	900	4.897E-05	3.730E-05	3.626E-05

Comparing activation energy barriers, E_a, with the maximal diffusion coefficient, D_0, for each compound in $Li_3InBr_{6-x}Cl_x$ showed correlation between the two terms. As a way to understand large variations in D_0, we consider the factors in the following equation:

$$D_0 = \frac{1}{6} f d^2 N_s v_o e^{\frac{S^M}{k_B}}$$

where f represents the Li correlation factor, d is jump length, N_s is number of neighboring sites, S^M is entropy of migration, and v_o is the jump attempt frequency. We find that as E_a increases, D_0 also increases, so diffusivity cannot be optimized by simply searching for the material with the smallest E_a (Fig. 3). Some of these values are taken from fitting data just at 800K and 900K for diffusivity in the high temperature regime.

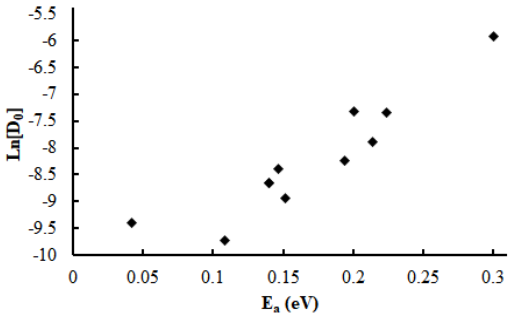

Figure 3. Correlation between E_a and D_0

Discussion

Through analysis of polar-covalent bond character and trends in structure and diffusivity at various volumes, temperatures, and compositions, we explain the high conductivity of nano-phase Br_3 and confirm the beneficial contribution of frustration to diffusivity. First we will discuss the nano-phase microstructure and then the effect of composition and volume on diffusion by comparing the Br_3 and Br_4 compositions.

Nano-phase:

Diffusion in Br_3 at 500K is significantly larger with the nano-phase microstructure than in the solid solution (Table 3) and explains the experimental trend in conductivity. The NP material has higher diffusivity at low temperature for two main reasons: 1. The expanded volume of the Cl region leads to a higher Li concentration and even higher Li diffusion in the Cl region, and 2. Compared to the solid solution, more Li diffuse in nano-phase microstructure channels, the interface between the Br and Cl regions. The NP likely has a slightly larger volume than the solid solution (which can be seen in the experimental volume hysteresis). The medium volume NP has higher diffusivity than the small (optimized) volume solid solution at all temperatures.

The larger volume Cl region compared to the relaxed volume leads to higher Li concentrations, as shown by the Ordinary (*Ord.*) % of Li in Table 5. Likewise, the Br region is compressed lowering the concentration in that region. In addition, the expansion and compression of the Cl and Br regions, leads to changes in activation energy barriers and more or less diffusion, respectively. As more space is made available between the 4112 and 4262 $Å^3$ volumes, there is an increase in jumping Li on the Br side, probably due to more free volume at the bottleneck (transition state) points. The increase in diffusion on the Br side as temperature increases is also supportive.

Table 5. % Ordinary and Jumping Li in NP Br_3

		Br-side		**Cl-side**	
Vol.	Temp.	*Ord.*	*Jump.*	*Ord.*	*Jump.*
4112	**700**	46.18	32.24	53.82	67.76
4262	**500**	44.63	36.01	55.37	63.99
	700	46.11	40.64	53.89	59.36
	800	46.06	42.13	53.94	57.87
	900	45.37	43.66	54.64	56.34
4389	**700**	45.98	39.89	54.02	60.11

In the solid solution, mixed Br/Cl neighbors leads to more diffusion (Table 2); in the nano-phase microstructure, mixed neighbors are found at the interface (channels). Thus, in the NP, we find more jumping Li in

the [010] vacancy rich channels, especially at low temperature. Figure 4 shows the percent difference of jumping versus ordinary Li in the channels is higher in the NP than in the solid solution. At low temperature the activation energy through the channel is lower, so more jumping will occur. As temperature increases, the difference between the microstructures decreases, as expected. Finally, the NP is as energetically favorable as the solid solution (see SI), lending support to a NP microstructure in the experimental conductivity measurement.

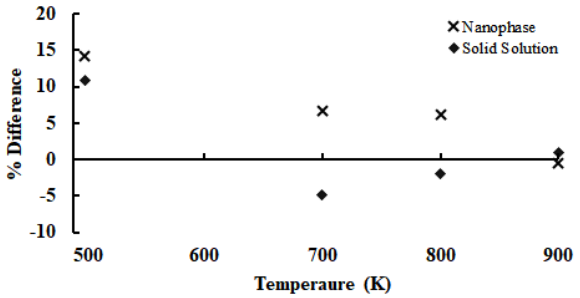

Figure 4. Percent difference between jumping versus average Li in channels.

Table SI.X. Relaxed Energies at 4262 Å^3

Energy	Br3-SS	Br6/Cl6 average	Br3-NP	Br6	Cl6
(eV E04)	-7.79	-7.79	-7.79	-7.44	-8.14

Dependence of Diffusivity on Composition - Br_3 vs Br_4:

Superionic conductors require low activation energy barriers, but high D_0 are also important. For example, even though Cl_6 has a smaller E_a than Br_3, Br_3 has a larger diffusion coefficient at 500K, due to its larger D_0. The D_0 is larger in the mixed halides compared to Cl_6 and Br_6. We posit that the higher D_0 in the mixed halides is due to an "ideal" bond length that causes maximum frustration. This type of frustration is the inability of the Li to form simultaneous polar-covalent bonds with all the anions in the octahedral site, leading to a higher jump attempt frequency, a flatter energy landscape, and thus a higher diffusivity.

In our previous analysis of bond character in Li_3InBr_6, a clear distinction between polar-covalent and ionic bond character was seen by plotting the Li-Br bond length and Li-Br-WC bond angle. Li-Br bonds with bond lengths greater than 2.6 Å and bond angles larger than 23° are ionic; bonds within those cutoffs are polar-covalent.

The ability of the Li to form simultaneous polar-covalent bonds depends on the size of the octahedral site, which is mostly determined by the volume of the cell. We define the size of the octahedral site by a single number (descriptor), the distance from an anion to the centroid of the site (centroid distance). The distance from the Li to the centroid depends on the volume of the cell and the Br/Cl composition. On average, the Li is not in the center of the octahedral site. If Li were in the center of the site, the average Li-anion bond length will equal the centroid distance. If the centroid distance is small, many Li-anion polar-covalent bonds are possible. In Li_3InBr_6, the centroid distance is much larger than 2.6 Å, so not every Br can form a polar-covalent bond with Li. Figure 5 shows Li offset from the centroid and trying to form simultaneous bonds with four Br neighbors.

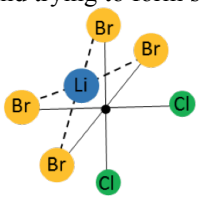

Figure 5. Li offset from octahedral centroid (black point) with four polar-covalent bonds to Br.

There can be bond frustration because the octahedral site is too large for the ionic radii (tetrahedral coordination is also favorable for Li and Br ionic radii), which leads to the centroid distance being larger than the minimum energy Li-anion distance. Additionally, the anion prefers a tetrahedral coordination of cations because there are four cation neighbors on average. Frustration increases upon mixing halides because 1. The Li-Cl polar-covalent bond is shorter than the Li-Br and 2. The volume does not decrease enough to compensate. We will show

how the Br_3 at 4262 Å^3 leads to the highest D_0. In addition, we will show that 3. Li jumps more often if there are more Br neighbors and 4. that the number of polar covalent bonds correlates with diffusivity, linking bond frustration and the jump attempt frequency. These analyses will demonstrate why mixed halides have higher D_0 than single-anion halides.

1. Polar covalent bond differences between Li-Br and Li-Cl

Shannon's ionic radii (effective) for Li, Cl, and Br in octahedral environments are 76nm (90nm), 181nm (167nm), and 196nm (182nm), respectively. Thus, Pauling's rules predict that Li-Cl will have octahedral coordination because the ratio between the cation and anion radii is between 0.414-0.732. Depending on whether the effective or crystal ionic radii, Pauling's rules predict Li-Br to have an octahedral or tetrahedral coordination, respectively[].

The smaller Cl ionic radius leads to more free volume and the shorter bond length for Li-Cl compared to Li-Br. Using our metric of comparing the Li-anion bond distance to the centroid distance, the large size of the Br_6 octahedral cage compared to the Cl6 octahedral cage is apparent. The difference between centroid distance and the Li-anion bond, henceforth called the Li-centroid distance, is 0.409 Å for Br6 and 0.199 Å for Cl6. In addition to the octahedral volume, the Li-centroid distance is affected by the strength of the polar-covalent bond.

According to Fajan's rules, the larger the anion, the more covalent the bond character, so Li-Br will have more polar-covalent character than Li-Cl bonds. We assess the polar covalent bond character by taking a probability density histogram of bond length and the Li-WC-anion angle (see Supplementary Information). These 2D histograms are difficult to visually compare, so we calculate the average bond distance at a given bond angle and visa versa (Figure 6). At angles smaller than 30°, the Li-Br and Li-Cl bond distances are distinct, no matter what the composition. The average Li-Br bond is around 2.75 Å and the average Li-Cl bond is around 2.6 Å. As the angle increases over 30°, all the bond distance start to converge, except for Cl6, indicating the ionic bond character. Interestingly, below a 12° bond angle, the Li-anion bond length does not change, indicating of polar-covalent bonds. Polar-covalent Li-Br bonds can occur at higher bond distances (around 2.8 Å) compared to Li-Cl (below 2.65 Å). Thus, Br can capture Li in a polar-covalent bond at larger distances.

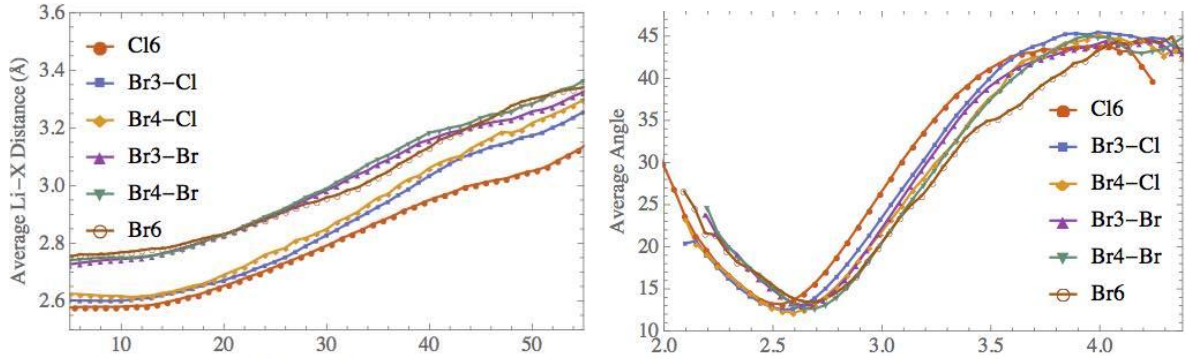

a. b.

Figure 6. Bond distances are for Li-halide and the bonding angle is Li-WC-halide: a) Average bond distance at a given angle and b) Average bond distance at a given angle.

In Li_3InBr_6, each Br only has 1-2 simultaneous polar-covalent bonds, but has 4 cation neighbors.[10] Some bonds are ionic because the Li is closer to other Br neighbors (in a polar-covalent bond). Br-anions can capture Li in a new polar-covalent bond, pulling the Li away from its current polar-covalent bond. The closer the Li is to the centroid, the more likely that neighboring Br can capture it. However, if the Li is very close to the centroid, like in Cl6, the anion neighbors can easily maximize simultaneous polar-covalent bond configurations, reducing frustration and lowering the jump attempt frequency. A frustrated octahedral site also increases the site energy and affects the activation energy barrier along with the size of the tetrahedral site.

Table 7. Difference, Δ, between the distance to octahedral/tetrahedral centroids from halide, with Li present in site, and ideal Li-Halide bond distances at 700 K.

		Octahedron			Tetrahedron			
	Vol. (Å^3)	Cntr$^+$	Li-Br/ Li-Cl	Δ	Cntr 2Br:2Cl	Cntr 4 X*	Li-Br/ Li-Cl	Δ

Li_3InBr_6	4389	3.091	2.682	-0.409	-	2.668	2.589	-0.079
$Li_3InBr_4Cl_2$	4389	2.849	2.576/ 2.401	-0.273/ -0.448	2.578	-	2.557/ 2.378	-0.021/ -0.200
	4262	2.773	2.587/ 2.404	-0.186/ -0.369	2.560	-	2.566/ 2.368	+0.006/ -0.192
	4112	2.768	2.665/ 2.475	-0.103/ -0.293	2.546, so small	-	2.594/ 2.397	***+0.048***/ -0.149
$Li_3InBr_3Cl_3$	4389	2.772	2.567/ 2.375	-0.205/ -0.397	2.580	-	2.533/ 2.340	-0.047/ -0.240
	4262	2.755	**2.551/ 2.450**	-0.204/ -0.305	2.532	-	2.547/ 2.359	+0.015/ -0.173
	4112	2.716	2.608/ 2.421	-0.108/ -0.295	2.512	-	2.507/ 2.350	-0.005/ -0.162
Li_3InCl_6	3638	2.612	2.413	-0.199	-	2.568	2.302	-0.266

[+] Br4:Cl2 for $Li_3InBr_4Cl_2$, and Br3:Cl3 for $Li_3InBr_3Cl_3$
*X = Br or Cl

2. The "ideal" bond length for frustration: Centroid- vs. Li-anion distance

We simulated each mixed compositions at three volumes to distinguish the effect of volume versus composition. As the volume increases, the Li moves farther away from the centroid (Table 7) because the Li-anion distance decreases, which is counter-intuitive from a purely ionic paradigm. We interpret this trend as showing that in the smaller volume cells, the Li-halide bond is stretched out by forming simultaneous polar-covalent bonds, especially with Br. As the volume increases, the Li cannot form simultaneous bonds as easily, so the primary Li-anion bond length shrinks. Between the medium and large volumes for Br3 (both larger than its optimized volume), the distance between the Li and the centroid does not change significantly. Br3 at the largest volume approaches an unphysical cell size and leads to outliers in the data. Note, a smaller Li-Br distance than 2.55 Å (from the medium volume simulation) is likely not preferable in the larger volume.

The Br3 composition at the medium volume leads to the "ideal" bond length to cause frustration. At the small, optimized volume, the Li makes multiple simultaneous polar-covalent bonds with Br in its octahedral site. The Li is relatively close to the centroid, with a distance of 0.11 Å. With a 3.6% increase in volume, the Li moves farther away from the centroid, frustrating the formation of multiple polar-covalent bonds with Br. However, the volume is still small enough that the Li can be captured by neighboring Br. The D_0 for this composition and volume is the highest of all the simulations, leading us to posit that frustration leads to a high jump attempt frequency, resulting in a larger D_0. Note we only consider frustration from the Br bonds because the Li has to be much closer to a Cl anion to form a bond with polar-covalent character. At the largest volume for Br3, the activation energy is very small, but the D_0 is also very small, because there is less frustration between competing Li-Br polar-covalent bonds.

Comparing Br4 to Br3, at the 4262 $Å^3$ volume, the Li is closer to the centroid in Br4, due to the ability to form more simultaneous polar covalent bonds because there are more Br neighbors. There is less frustration (and less free volume) in the Br4 compared to the Br3 at this volume, which is reflected in the larger D_0 for Br3 than Br4 (Table 3). At the largest volume, the Br4 now has "ideal" bond lengths for frustration, leading to the highest D_0 for the Br4 compositions.

3. More Br neighbors = more jumps

Having multiple frustrated polar-covalent bonds leads to frustration, which we posit leads to a higher jump attempt frequency. Thus Li with more Br neighbors should jump more than Li with fewer Br neighbors. The Br and Cl are distributed randomly in the cells, so some sites have more Br neighbors than others, even in the Br3 composition. By counting the number of Br neighbors that jumping Li have, we find that more Br neighbors lead to a higher likelihood for jumping. Our analysis proceeds as follows:

1. Calculate the percentage of Li with more than 3 Br neighbors, 3 Br neighbors, and less than 3 Br neighbors.
2. Calculate the difference in percentage of Li with more than 3 Br neighbors versus less than 3 Br neighbors %(w/ more Br).
3. Compare this percentage difference %(w/ more Br) for jumping Li to the the average values for Li with more Br in the simulation = %(jumping w/ more Br).

For Br3 with its optimized volume at 500K, %(jumping w/ more Br) = 11%. Jumping Li are 11% more likely to have more Br neighbors than the average Li (Figure 7 and Table 8). As the volume increases, this percentage decreases from 11% to 6% to 5%, but jumping Li are still more likely to have excess Br neighbors. At 700 K, jumping Li still prefer excess Br neighbors, but the maximum percentage difference is 5.6%. As the temperature increases to 800 K and 900 K, the average percentage difference at the three different volumes also increases until at 900 K there seems to be no preference for excess Br or Cl neighbors (see Table in SI).

One might expect that more Cl neighbors would lead to a higher likelihood of jumping because there would be more free volume at the bottleneck point, but we find the opposite. The surprising results support the idea that

frustration is created by Br competing for polar-covalent bonds in the octahedral site. The frustrated octahedral sites will have fewer polar covalent bonds than the smaller less-frustrated sites.

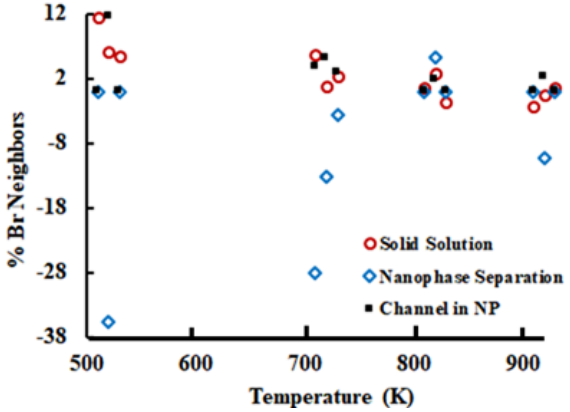

Figure 7. Li with more Br neighbors vs Cl neighbors (jumping minus average). Circles, diamonds, and squares represent solid solution, nano-phase separation, and Li in NP channels respectively.

Table 8. Percent Br neighbors to jumping Li

$Li_3InBr_3Cl_3$	Temp (K)	4112 Å^3	4262 Å^3	4389 Å^3	channel nano
Solid solution	**500**	11.5%	6.2%	5.4%	-
	700	5.6%	0.9%	2.3%	-
	800	0.6%	2.9%	-1.6%	-
	900	-2.4%	-0.6%	0.6%	-
Nanophase	**500**		-35.7%		11.6%
	700	-28.2%	-13.1%	-3.7%	3.8, 5.2, 2.9%
	800		5.2%		1.8%%
	900		-10.3%		2.2%

4. Polar-covalent bond percentage supports frustration

Using the Wannier analysis, we are able to count the percentage of polar-covalent bonds, compared to the percentage of free WCs and ionic bonds (Figure 8). Here we plot the percentage of polar-covalent Li-Br bonds with respect to temperature and volume for Br3 and Br4. In Fig. 8, the data at larger volumes is shifted right slightly at each temperature. The Br6 has a larger percentage of polar-covalent bonds and the Cl6 has a smaller percentage.

The systems with the largest percentage of polar covalent bonds are Br3 at 4112 Å^3, Br4 at 4262 Å^3 and Br4 at 4389 Å^3, which is perhaps not surprising because there are more Br in the Br4 compositions, making multiple simultaneous Li-Br polar-covalent bonds more likely. As noted before, the Br4 at 4112 Å^3 is too small for the Br/Cl ratio, so shows unusual behavior as temperature is increased (blue filled diamond). Interestingly Br3 at 4112 Å^3 has the largest percentage of polar-covalent bonds - indicating that it can keep multiple simultaneous polar covalent bonds, with less frustration.

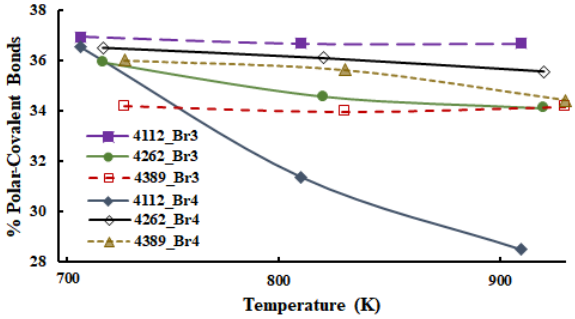

Figure 8. Percentage of polar-covalent bonds.

Comparing Br3 at 4262 Å^3 and 4389 Å^3 shows how the "ideal" bond length and volume leads to frustration. Br3 at 4262 Å^3 (green) has a relatively high percentage of polar covalent bonds at 700 K, but this value drops off quickly with temperature, as the thermal energy overcomes the the polar-covalent bond energy. At the largest Br3 volume (red), there are few polar covalent bonds compared to the other systems at 700K because the volume is simply too big. Interestingly, the percentage of polar covalent bonds at the large volume converges for Br3 and Br4 at 900K. The composition no longer plays a role at this large temperature and volume.

The trend with temperature of percentage of polar covalent bonds for Br3 at 4262 Å^3 sheds light on the extraordinarily high D_0 for this system.

Activation energy barrier: Trends between D_0 and E_a

We find a strong trend between the activation energy barrier and D_0 (Figure 3). Since a large D_0 and a small E_a is desired for superionic electrolytes, one cannot simply optimize E_a. The size of the tetrahedral site can be used to explain the trends in E_a. The frustration in the tetrahedral site also stems from a mismatch between the volume of the site and the energetically preferred Li-anion bond length.

The activation energy for ion conduction in solids often decreases with increasing volume because there is more free volume at the transition state or bottle-neck. We find that that neither Br4 nor Br3 follows this trend, though the Br4 simulation with the smallest volume has a very large activation energy barrier, probably due to bottleneck problems. Br4 has the smallest activation energy barrier with a volume of 4262 Å^3 rather than 4389 Å^3 due to stabilization of the tetrahedral site at the medium volume, despite to frustration (destabilization) of the octahedral site at the large volume.

In contrast, Br3 has the highest E_a at the 4262 Å^3 volume. For Br3, the large volume probably has a low E_a due to the free volume at the bottleneck point. The smallest volume has an optimal tetrahedral site, giving a low E_a. Unusually, the tetrahedral site at the 4262 Å^3 volume seems too small, leading to the high E_a. The tetrahedral site seems to dictate E_a over the octahedral site, which affects D_0 more.

Table 7 shows that the tetrahedral site is always too large for the Cl-Li bonds in the mixed systems. The Li-centroid distance is always negative, indicating the Li is closer to the Cl than the centroid. For Br6, the Li-Br is optimized in tetrahedral site, confirming the lack of preference for octahedral coordination in Li_3InBr_6.

Conclusions

In conclusion, we explain the experimental trend in the conductivity with composition by showing that the $Li_3InBr_3Cl_3$ has a nano-phase separated microstructure rather than a solid solution. The nano-phase microstructure is supported by the equivalence in calculated cell energy between the nanophase and solid solution. We find that at 500 K, the nanophase has an order of magnitude higher diffusion than the solid solution and is 3X larger than the $Li_3InBr_4Cl_2$.

Calculation of E_a and D_0 across varying Cl-Br compositions highlights the importance of a low E_a **and** a large D_0 for superionic diffusivity. We find a large D_0 can be understood through bond frustration and controlled

through isovalent substitution and volume. The "ideal" Li-Br bond length to maximize frustration and thus the jump attempt frequency occurs in $Li_3InBr_3Cl_3$ at a slightly larger volume than the optimized volume due to competition between polar-covalent bonds with with six Br in the octahedral site. Frustration in bonds, coupled with a low E_a, leads to superionic diffusion.

Acknowledgements
The authors acknowledge Lawrence Livermore National Laboratory (LLNL) for Grand Challenge supercomputer cycles and support from LDRD 15-ER-022

References

1) Thangadurai, V., Narayanan, S., Pinzaru, D. *Chemical Society Reviews*. 43(14): 4714 (2014).
2) Xu, M., Park, M.S., Lee, J.M., Kim, T.Y., Park, Y.S. and Ma, E. *Physical Review B*. *85*(5), p.052301 (2012).
3) Murugan, R., Thangadurai, V. and Weppner, W., *Angewandte Chemie International Edition*. *46*(41), 7778 (2007).
4) Richards, W.D., Tsujimura, T., Miara, L.J., Wang, Y., Kim, J.C., Ong, S.P., Uechi, I., Suzuki, N. and Ceder, G. *Nature communications*. *7* (2016).
5) Ortiz, G.F., López, M.C., Lavela, P., Vidal-Abarca, C. and Tirado, J.L. *Solid State Ionics*. *262*, 573 (2014).
6) Arbi, K., Bucheli, W., Jiménez, R. and Sanz, J. *Journal of the European Ceramic Society*. *35*(5), 1477 (2015).
7) Zhao, Y. and Daemen, L.L. *Journal of the American Chemical Society*. *134*(36), 15042 (2012).
8) Fang, H., Wang, S., Liu, J., Sun, Q. and Jena, P. *Journal of Materials Chemistry A*. (2017).
9) Kamaya, N., Homma, K., Yamakawa, Y., Hirayama, M., Kanno, R., Yonemura, M., Kamiyama, T., Kato, Y., Hama, S., Kawamoto, K. and Mitsui, A. *Nature materials*. *10*(9), 682 (2011).
10) Adelstein, N. and Wood, B.C. *Chemistry of Materials*. *28*(20), 7218 (2016).
11) Fajans, K. and Joos, G. *Zeitschrift für Physik*. *23*(1), 1 (1924).
12) Tomita, Y., Matsushita, H., Kobayashi, K., Maeda, Y. and Yamada, K. *Solid State Ionics*. *179*(21), 867 (2008).
13) Born, M. and Oppenheimer, R. Zur quantentheorie der molekeln. *Annalen der Physik*. *389*(20), pp.457 (1927).
14) Giannozzi, P., Baroni, S., Bonini, N., Calandra, M., Car, R., Cavazzoni, C., Ceresoli, D., Chiarotti, G.L., Cococcioni, M., Dabo, I., Dal Corso, A. *Journal of physics: Condensed matter*. *21*(39), p.395502 (2009).
15) Vanderbilt, D. *Physical Review B*. *41*(11), 7892 (1990).
16) Perdew, J.P., Burke, K. and Ernzerhof, M. *Physical review letters*. *77*(18), 3865 (1996).
17) Mostofi, A.A., Yates, J.R., Lee, Y.S., Souza, I., Vanderbilt, D. and Marzari, N. *Computer physics communications*. *178*(9), 685 (2008).
18) Marzari, N. and Vanderbilt, D. *Physical review B*. *56*(20), 12847 (1997).
19) Souza, I., Marzari, N. and Vanderbilt, D. *Physical Review B*. *65*(3), 035109 (2001).
20) Tomita, Y., Matsushita, H., Kobayashi, K., Maeda, Y. and Yamada, K. *Solid State Ionics*. *179*(21), 867 (20

08).